EXPERIMENTAL INVESTIGATION OF PARTICLE-WAKE INTERACTIONS BASED ON FREELY FALLING FINITE PARTICLES

Yi Hui Tee, James R. Dawson and R. Jason Hearst
Department of Energy and Process Engineering
Norwegian University of Science and Technology
Trondheim, Norway
yi.h.tee@ntnu.no, james.r.dawson@ntnu.no, jason.hearst@ntnu.no

ABSTRACT

Research on freely falling particles has primarily focused on wake dynamics and vortex shedding of individual particles in quiescent flow. When these particles fall collectively, the wakes of surrounding particles alter the flow fields. Hence we conducted volumetric experiments to investigate how the settling and wake dynamics of particles are affected by the wakes of other settling particles. Negatively buoyant 12 mm particles of various shapes are first released individually into quiescent water. Then, the particles are released individually into the bulk wakes of 20 mono-dispersed particles. Using four high-speed cameras and LEDs, we simultaneously capture both 3D particle and fluid motions within an imaging domain measuring 90 mm × 90 mm × 40 mm. Our results show that all trailing particles settling through the bulk wakes gain additional downward momentum from the turbulent wakes, falling faster than in the quiescent flow. Upstream of the particle, the vortices in the bulk wake interact with the developing shear layer along the particle. The wake downstream of the trailing particle also appears more chaotic than that in a quiescent flow.

INTRODUCTION

Freely falling collective particles exhibit complex dynamics due to the interactions of their wakes with the surrounding fluid and particles. Previous studies have primarily focused on wake dynamics and vortex shedding of individual particles to characterize their shape-dependent trajectories due to the effects such as density ratios and particle Reynolds numbers (Ern *et al.*, 2012). For non-spherical particles, instead of a steady descent, they may tumble, flutter, or undergo chaotic motion. These motions are influenced by their Reynolds numbers and moments of inertia, which are determined by their shapes and aspect ratios. However, when these particles fall in bulk, the flow fields are perturbed by the wakes of neighboring particles, affecting the settling dynamics of the trailing particles. Classical studies such as Fortes *et al.* (1987) on fluidization have observed how the inertial effects associated with wakes can lead to the capture of one particle in the wake of another.

Nevertheless, considering the three-dimensional nature of the wake structures, volumetric studies on the flow around falling particles have been limited due to experimental challenges. Some advanced measurements include Adhikari & Longmire (2012), who studied the flow around moving objects using Tomographic Particle Image Velocimetry (PIV). Here, the moving objects were reconstructed separately from the tracer particles using visual hull reconstruction. Meanwhile, Esteban *et al.* (2019) studied the flow around falling polygonal particles using a combination of non-time-resolved volumetric V3V camera systems with separate high-speed camera imaging from two orthogonal directions. More recently, Wieneke (2023) studied the flow around a stationary cylinder using a Lagrangian particle tracking (3D-LPT) algorithm in a volumetric measurement. The cylinder was reconstructed using Iterative Particle Reconstruction (IPR), which was used in Shake-The-Box (STB) in DaVis by LaVision GmbH (Schanz *et al.*, 2016).

In this study, we conduct volumetric experiments to investigate how the particle settling and wake dynamics are affected by the wake structures from particles falling collectively. The research goal is to identify particle-wake interactions when particle Reynolds numbers are large, on the order of 10^3. This is important for the understanding of the transport of large sediments, macroplastic pollutants, or other natural particles in our environment where the particles have been traditionally modelled as point-masses in simulations of particle-laden flow at high volume-fraction (Brandt & Coletti, 2022).

METHODOLOGY

To investigate the effects of particle shapes on the settling dynamics, we fabricated particles with four distinct geometries but the same mass and volume: a sphere, a cuboid, a circular cylinder, and a square cylinder. All particles were printed using resin with a solid-to-fluid density ratio (ρ_s/ρ_f) of 1.15. The sphere has a diameter of $l_1 = 12$ mm, while the other particles have a length of $l_1 = 12$ mm along their longest axis and a thickness of l_2 along their shortest axis. By keeping l_1 constant, the values of l_2 were chosen such that the volume and mass of each particle are equal to those of the sphere. Consequently, the particle Reynolds numbers, defined as $Re_p = l_1|\vec{U}|/\nu$, vary only with the particle settling velocity ($|\vec{U}|$). Here, ν refers to the kinematic viscosity of water. The detailed parameters of the particles as shown in Figure 1*a* can be found in Table 1.

The experiments were performed in an open hexagonal acrylic tank with a maximum length, width, and height of 0.61 m × 0.51 m × 0.52 m, respectively. The tank was filled with water up to 0.4 m. These negatively buoyant particles were first released individually in a quiescent liquid below the water surface and allowed to fall. To avoid any side wall effect, the particles were released at least $7l_1$ from the nearest sidewalls. Then, the particles were released individually into the bulk wake of monodispersed particles of the same sizes and

Figure 1: Experimental details. *(a)* Schematic and photo of $l_1 = 12$ mm particles. Clockwise from top left: sphere, flat cuboid, square cylinder, and circular cylinder. *(b)* Schematic illustration of the volumetric measurements using four high-speed cameras and LEDs.

Table 1: Particle parameters.

Particle	$l_1\,[mm]$	$l_2\,[mm]$	$Re_p = l_1\lvert\vec{U}\rvert/\nu$
Sphere	12	-	2400
Flat Cuboid	12	6.3	1300
Square cylinder	12	8.7	1550
Circular cylinder	12	9.8	1900

shapes to study the effect of wake interactions on the settling dynamics. These results were compared with those obtained from single-particle falling experiments.

To capture both the particle dynamics and fluid wake simultaneously, we set up a time-resolved volumetric measurement using four Photron FASTCAM Mini WX100 4MP high-speed cameras with 2048 $\times$ 2048 pixel resolution. The cameras were arranged on the front side of the hexagonal tank spanning over 110° as shown in Figure 1*b*. All cameras were mounted with Sigma 105 mm lens (f/22) with scheimpflugs to improve focus. Four units of GSVITEC MultiLED QT pulsed LEDs with 15° lens were used to illuminate the measurement domain from the top. The water was seeded with 40 μm Dynoseeds. Here, the imaging volume was centered at $20l_1$ from the water surface and $13l_1$ above the bottom wall to capture the steady particle motion while avoiding any possible boundary effects. This results in a reconstructed domain measuring 90 mm $\times$ 90 mm $\times$ 40 mm in the x, y, and z direction as shown in Figure 1*b*. The sampling rate was varied between 500 Hz to 1000 Hz depending on the particle settling velocity to prevent particle streaks in the wake regions. The image resolution was 0.053 mm/pixel.

The acquisition and processing were performed using DaVis 10.2. For classic multi-camera calibration, the LaVision plate (type 20) was traversed in the z-direction through five positions. Then, a self-calibration was performed using 300 images. Here, we first normalized the image intensity distributions across all cameras. Since the particle appeared as a very bright spot in the images, using the image segmentation algorithm in DaVis 10.2, the big particles (objects) and tracers were separated into two different image sets. With the object masked from the tracer particles, the fluid flow fields were processed using STB followed by the Fine-Scale Reconstruction (VIC#) to convert the Lagrangian particle tracks to Eulerian fields (Jeon *et al.*, 2018). Meanwhile, we reconstruct the falling particles using IPR as explained above. This generates point clouds of the particle that we fit with a sphere or a cuboid to obtain the centroid location.

RESULTS AND DISCUSSION

The particles of various geometries have different frontal areas that affect the drag that they encounter while falling. Since these particles have the same density and mass, in a quiescent flow, as plotted in Figure 2 as dashed lines, the sphere (black) settles the fastest, while the flat cuboid settles the slowest (red). The rounded surface of the circular cylinder (blue) also causes it to sink at a higher velocity than the square cylinder (green). This results in Re_p ranging from 1300 to 2400 (see Table 1), where all particles are in the vortex shedding regime.

If we compare these settling velocities with those of a particle falling into the bulk wake of 20 particles of the same size and shape, for all four geometries plotted as solid lines in Figure 2, they sink faster than in the quiescent flow. In the case where a sphere is falling into the bulk wakes of 20 flat cuboids, the results (black dashed-dot lines) show that they settle at approximately the same velocity as the spheres that are falling into the bulk wakes of 20 spheres. This suggests that the effect of geometries on the bulk wake of the collective particle is negligible on the sphere settling velocity.

To understand the increment in the particle settling velocity, we computed the instantaneous probability density function of the flow velocity within the measurement volume in Figure 3. At the instance right before the sphere enters the top of the measurement volume in a quiescent flow, the PDFs plotted in red suggest that all fluid velocities (U, V and W for x, y and z) center about zero, indicating that the flow is quiescent-like. On the other hand, at the instance right after all 20 spheres have fallen entirely out from the bottom of the field of view, the PDFs plotted in black show longer tails, spreading over a wider velocity range. For the wall-normal velocity, the falling of the collective particles induces a stronger downward momentum, and the PDF is skewed toward the negative values. For this example, after approximately 3.2 s, right before the trailing sphere enters the measurement volume, the PDFs plotted in blue show a similar distribution for U and W. Meanwhile, the negatively skewed V shifts and centers around -0.02 ms^{-1}. If we compare this to the velocity increment reported in Figure 2, they are of a similar magnitude. This shows that the trailing particles gain additional momentum from these turbulent wakes and thus settle faster.

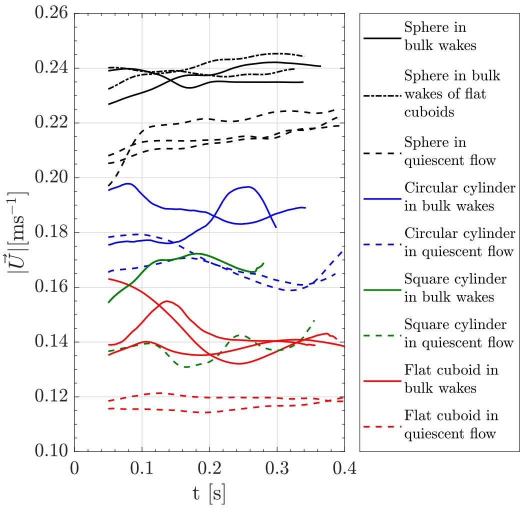

Figure 2: Superposition of sphere settling velocity curves from multiple runs, plotted against time. Dashed lines indicate particles falling into a quiescent flow while solid lines indicate particles falling into the bulk wakes. Black, blue, green and red represent sphere, circular cylinder, square cylinder and flat cuboid, respectively. Black dashed-dot lines indicate a sphere falling into the bulk wakes of the flat cuboids.

Based on the examples mentioned above, we first consider the three-dimensional vortices shed from a sphere in a quiescent flow. Figures 4 and 5 show the isosurfaces of the instantaneous vortical structures visualized using the magnitude of the Lamb vector $|\vec{L}|$ and the square of the swirling strength λ_{ci}^2, respectively. The Lamb vector is defined as the curl of the velocity and the vorticity ($-\vec{L} = \vec{U} \times \vec{\omega}$) and the magnitude is computed by taking the square root of the sum of the square of the Lamb vector components. It originates from the material derivative of the Navier-Stokes equation (vorticity equation) as the convective acceleration (Wu *et al.*, 2006). Meanwhile, the swirling strength plotted in Figure 5 is computed from the imaginary part of the complex eigenvalues of the local velocity gradient tensor. It is one of the several commonly used methods to identify vortex structures (Zhou *et al.*, 1999). The isosurfaces are plotted based on a threshold value of $|\vec{L}| = 0.15$ ms^{-2} and $\lambda_{ci}^2 = 6$ s^{-2}, respectively. The color plotted on top of the isosurfaces shows the spanwise vorticity ω_z normalized by the sphere diameter and the settling velocity in a quiescent flow.

As the sphere falls into a quiescent flow, distinct hairpin-like vortices with spanwise vorticity of opposite directions are shed downstream as shown by the isosurfaces of both $|\vec{L}|$ and λ_{ci}^2. In this context, dye visualization experiments by Sakamoto & Haniu (1990) show that for a sphere in uniform flow, when $Re_p > 300$, hairpin-shaped vortices begin to be periodically shed from the sphere, forming a laminar wake. As Re_p increases beyond 800, the laminar shear layer begins to shed periodically from the sphere and the wake flow becomes more turbulent. The direct numerical simulation by Rodriguez *et al.* (2011) also confirmed that for a sphere within the sub-critical Reynolds numbers of 3700, the instability in the laminar boundary layer that separates from the sphere causes the vortex sheets to roll up and transition into a turbulent wake. Thus the shed vortices observed in Figures 4 and 5 resemble the hairpin vortices in the turbulent wake.

For a sphere falling into the bulk wakes of 20 spheres of the same size, the isosurfaces of $|\vec{L}|$ plotted in Figure 6 using the same threshold as in Figure 4 show that the sphere is enveloped by cylindrical vortices or vortex tubes starting from almost one diameter upstream of the sphere. The swirling strength plotted in Figure 7 clearly illustrates that the trailing sphere falls into a chaotic region of vortices shed from the leading bulk particles. As compared to the shear layer observed for a sphere in quiescent flow, there are longer, extended vortices upstream of the sphere, connecting to the shear layer. In addition, the distinct hairpin structures that were observed earlier in Figure 7 for a sphere settling in quiescent flow are not as well identifiable here. A similar observation was reported in the DNS by Bagchi & Balachandar (2004) on a stationary, isolated sphere in an isotropic turbulent flow at $Re_p = 610$ where the coherent structures in the wake became irregular and dissipated quickly downstream (see also Wu & Faeth, 1993). However, it was noted that the downstream shear layers shed from the sphere were instead shortened and broken into smaller vortices. Nevertheless, the results suggest that the turbulent wakes of the leading collective particles interact with the shear layer and disrupt the hairpin vortices shed from the trailing sphere.

For a flat cuboid settling in a quiescent flow, the results in Figure 8 show that the particle is shedding long, streaky structures. The wake also meanders as it falls. Here, the particle flutters, rocks, or oscillates left and right, without tumbling or overturning. Meanwhile, the circular cylinder tumbles while falling (not shown here). The Reynolds number and moment of inertia phase diagram for rectangular plates reported by Smith (1971), plotted similarly to that for circular disks measured by Willmarth *et al.* (1964), shows that when $Re_p = 1300$ and dimensionless moment of inertia $I^* = 8\rho_s l_2 (l_1^2 + l_2^2)/3\pi\rho_f l_1^3 = 0.65$ (see Andersen *et al.*, 2005), the flat cuboid is within the stage of rocking motion. This rocking or fluttering motion matches well with our observation.

When we release a flat cuboid into the bulk wakes, the meandering shed vortices also interact with the surrounding vortices (see Figure 9). Within the measurement volume, it appears that the interaction between the bulk wake and the shear layer shedding from the flat cuboid causes the flat cuboid to flutter more violently, at a higher amplitude, than in the quiescent flow. Finally, if we consider the case where a sphere is falling into the bulk wakes of the flat cuboids (see Figure 10), we observe a similar pattern as in Figure 7, where the shear layer interacts with the upstream vortices. Downstream of the sphere, the hairpin vortex loops are vaguely visible, but the wake is more chaotic. Since the sphere is shedding within a sub-critical Reynolds number range where the shear layer is transitioning from laminar to turbulence (Rodriguez *et al.*, 2011), it is possible that the presence of bulk wake promotes an early onset of the transition. However, as aforementioned, the interaction of the trailing sphere with different structures of shed vortices does not seem to affect the settling velocity significantly. With the present data sets, more quantitative analysis on the orientation of the settling particle and wake analysis will be performed in the future to investigate these observations in detail.

CONCLUSIONS

We conducted volumetric experiments to investigate how the particle settling dynamics and shed vortices are affected by the bulk wake left over by the leading collective particles. Four high-speed cameras were set up to capture both the settling particle and the surrounding flow fields within the terminal velocity regime. Four 12 mm particles of different geome-

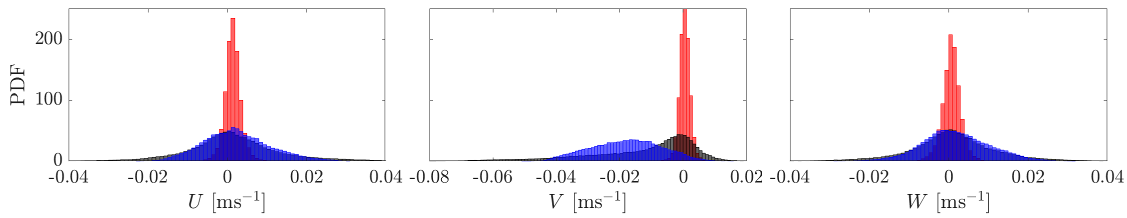

Figure 3: Instantaneous PDF of the three-component fluid velocity at the instances right before a sphere falling into the quiescent flow enters the top field of view (red), after 20 collective spheres moved entirely out from the bottom field of view (black) and before a trailing particle falling into the bulk wake enters the top field of view (blue).

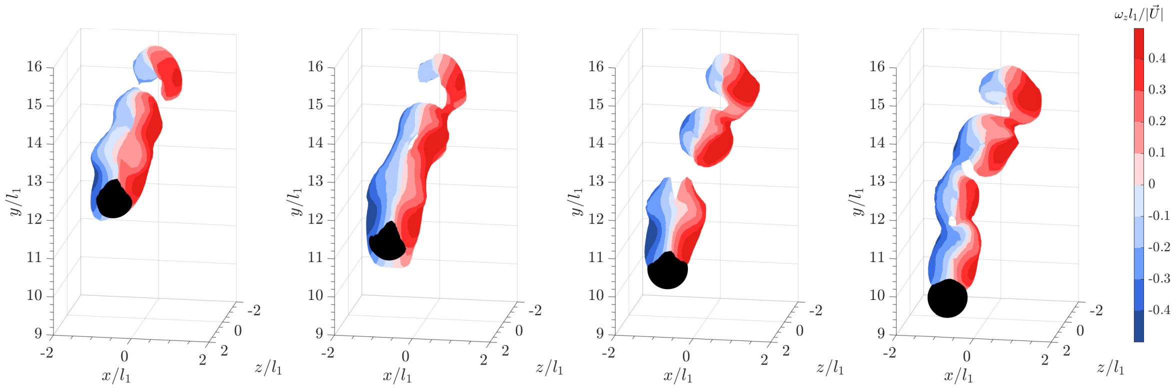

Figure 4: Time series of a sphere falling into a quiescent flow from left to right: isosurface plots of the instantaneous vortical structures visualized using the magnitude of the Lamb vector, $|\vec{L}| = 0.15$. Color represents spanwise vorticity normalized by sphere diameter and settling velocity in a quiescent flow.

tries (sphere, circular cylinder, square cylinder and flat cuboid) were released individually into the bulk wake of 20 collective particles. The results are compared to those in a quiescent flow. All particles of various geometries sink faster in the bulk wakes due to the downward vertical momentum induced by the turbulent bulk wakes. Regardless of the shape of the collective particles, the sphere sinks at a similar velocity in the bulk wakes of both spheres and flat cuboids. The hairpin vortices shed from a sphere at $Re_p = 2400$ in a quiescent flow resemble those reported in the literature within the sub-critical Reynolds number range. As the sphere sinks into the bulk wake, upstream of the particle, the vortices in the bulk wake interact with the shear layer that develops along the particle. Downstream of the sphere, the wake becomes more chaotic. Similar vortex interactions are observed for the flat cuboids. For this particle, the fluttering motion causes the wake to meander. Although the particle settling regime for flat cuboids in both quiescent flow and bulk wakes remains unchanged within the phase diagram, the vortex interactions likely cause the flat cuboid to flutter more unstably and over a larger amplitude in the latter.

REFERENCES

Adhikari, D & Longmire, E K 2012 Visual hull method for tomographic PIV measurement of flow around moving objects. *Experiments in fluids* **53**, 943–964.

Andersen, A, Pesavento, U & Wang, Z Jane 2005 Unsteady aerodynamics of fluttering and tumbling plates. *Journal of Fluid Mechanics* **541**, 65–90.

Bagchi, Prosenjit & Balachandar, S 2004 Response of the wake of an isolated particle to an isotropic turbulent flow. *Journal of Fluid Mechanics* **518**, 95–123.

Brandt, L & Coletti, F 2022 Particle-laden turbulence: progress and perspectives. *Annual Review of Fluid Mechanics* **54**, 159–189.

Ern, P, Risso, F, Fabre, D & Magnaudet, J 2012 Wake-induced oscillatory paths of bodies freely rising or falling in fluids. *Annual Review of Fluid Mechanics* **44**, 97–121.

Esteban, L B, Shrimpton, J & Ganapathisubramani, B 2019 Three dimensional wakes of freely falling planar polygons. *Experiments in Fluids* **60**, 1–12.

Fortes, A F, Joseph, D D & Lundgren, T S 1987 Nonlinear mechanics of fluidization of beds of spherical particles. *Journal of Fluid Mechanics* **177**, 467–483.

Jeon, Y J, Schneiders, J F G, Müller, M, Michaelis, D & Wieneke, B 2018 4D flow field reconstruction from particle tracks by VIC+ with additional constraints and multigrid approximation. In *Proceedings 18th International Symposium on Flow Visualization*. ETH Zurich, Switzerland.

Rodriguez, Ivette, Borell, Ricard, Lehmkuhl, Oriol, Segarra, Carlos D Perez & Oliva, Assensi 2011 Direct numerical simulation of the flow over a sphere at Re= 3700. *Journal of Fluid Mechanics* **679**, 263–287.

Sakamoto, H. & Haniu, H. 1990 A Study on Vortex Shedding From Spheres in a Uniform Flow. *Journal of Fluids Engineering* **112** (4), 386–392.

Schanz, D, Gesemann, S & Schröder, A 2016 Shake-The-Box: Lagrangian particle tracking at high particle image densities. *Experiments in fluids* **57**, 1–27.

Smith, EH 1971 Autorotating wings: an experimental investigation. *Journal of Fluid Mechanics* **50** (3), 513–534.

Wieneke, B 2023 3D-LPT in the presence of obstructing objects. In *Proceedings of the 15th International Symposium on Particle Image Velocimetry*. San Diego, California, U.S.A.

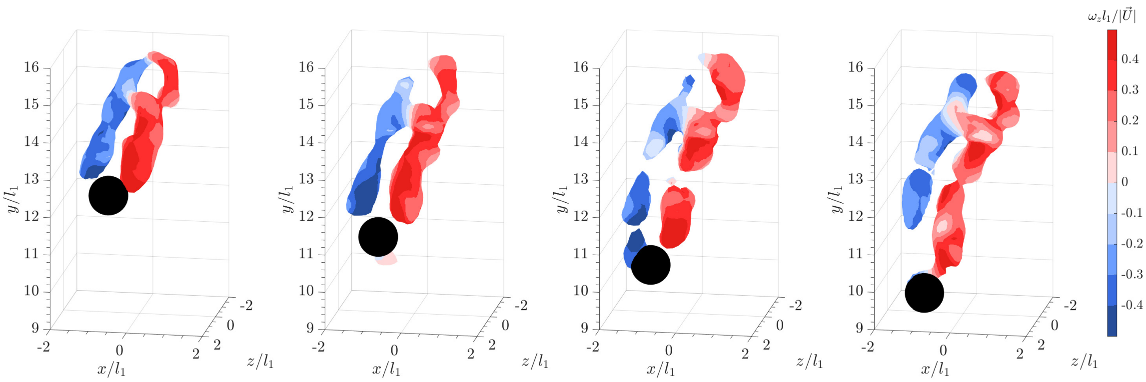

Figure 5: Time series of a sphere falling into a quiescent flow from left to right: isosurface plots of the instantaneous vortical structures visualized using the square of the swirling strength, $\lambda_{ci}^2 = 6$. Color represents spanwise vorticity normalized by sphere diameter and settling velocity in a quiescent flow.

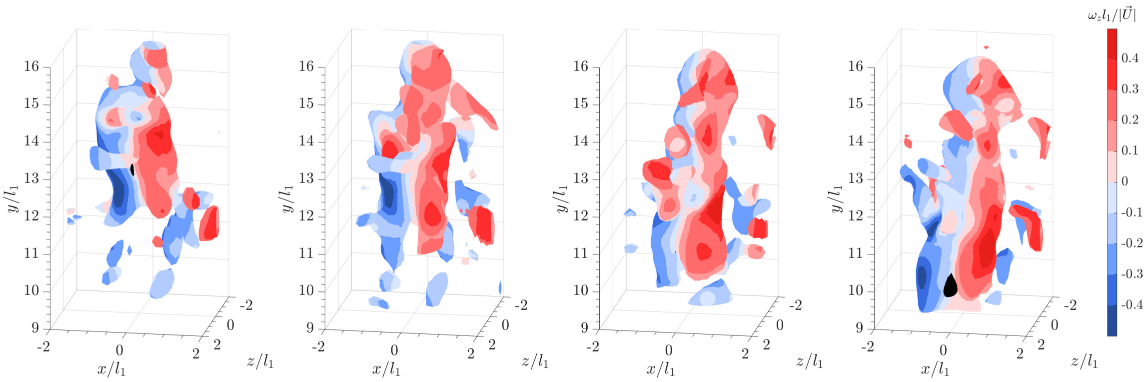

Figure 6: Time series of a sphere falling into the wake of leading collective particles from left to right: isosurface plots of the instantaneous vortical structures visualized using the magnitude of the Lamb vector, $|\vec{L}| = 0.15$. Color represents spanwise vorticity normalized by sphere diameter and settling velocity in a quiescent flow.

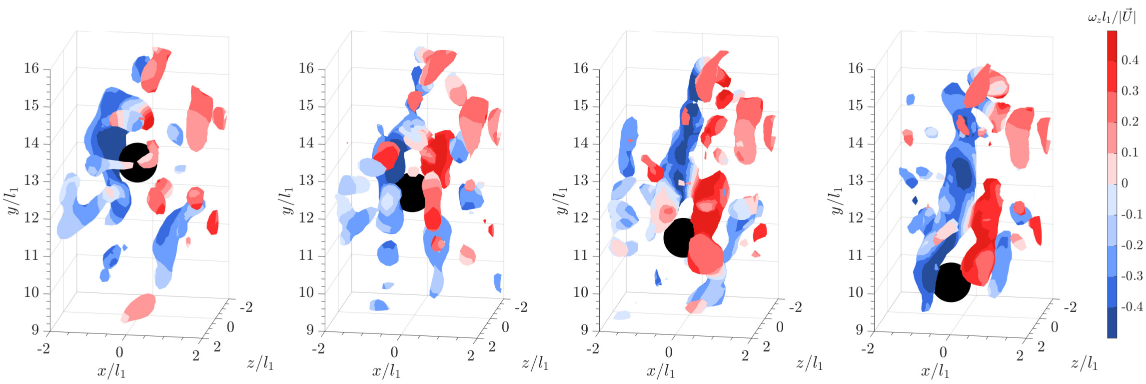

Figure 7: Time series of a sphere falling into the wake of leading collective particles from left to right: isosurface plots of the instantaneous vortical structures visualized using the square of the swirling strength, $\lambda_{ci}^2 = 6$. Color represents spanwise vorticity normalized by sphere diameter and settling velocity in a quiescent flow.

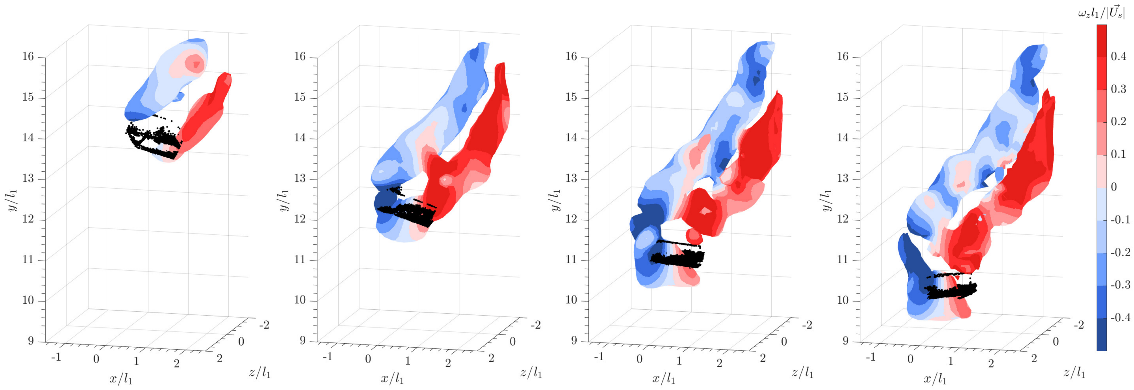

Figure 8: Time series of a flat cuboid falling into a quiescent flow from left to right: isosurface plots of the instantaneous vortical structures visualized using the square of the swirling strength, $\lambda_{ci}^2 = 6$. Color represents spanwise vorticity normalized by sphere diameter and sphere settling velocity ($|\vec{U}_s|$) in a quiescent flow.

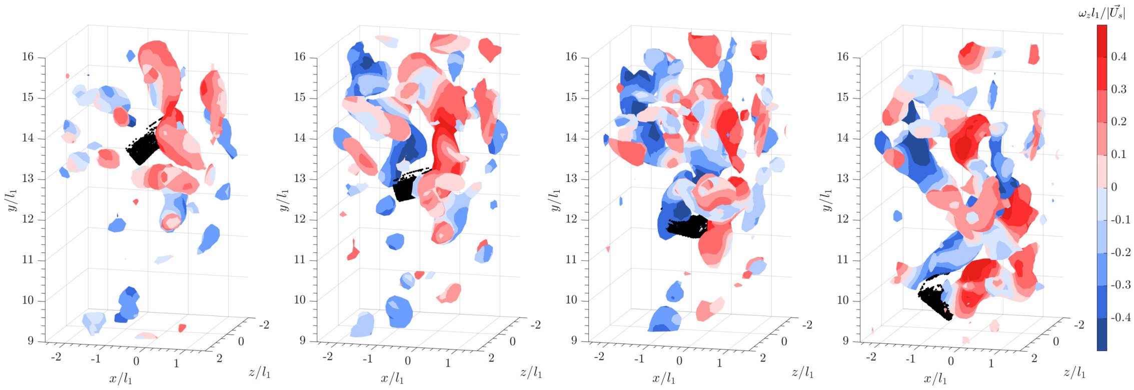

Figure 9: Time series of a flat cuboid falling into the wake of leading collective particles from left to right: isosurface plots of the instantaneous vortical structures visualized using the square of the swirling strength, $\lambda_{ci}^2 = 6$. Color represents spanwise vorticity normalized by sphere diameter and sphere settling velocity ($|\vec{U}_s|$) in a quiescent flow.

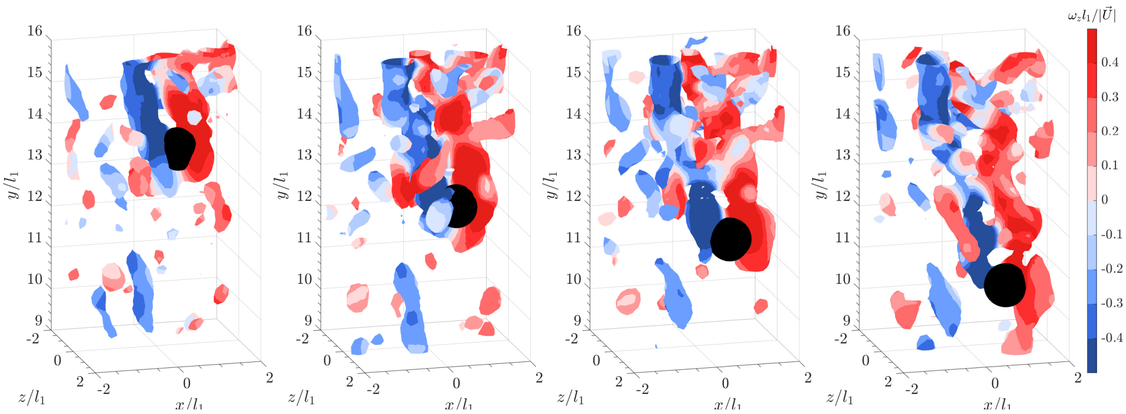

Figure 10: Time series of a sphere falling into the wake of 20 leading flat cuboids from left to right: isosurface plots of the instantaneous vortical structures visualized using the square of the swirling strength, $\lambda_{ci}^2 = 6$. Color represents spanwise vorticity normalized by sphere diameter and settling velocity in a quiescent flow.

Willmarth, William W., Hawk, Norman E. & Harvey, Robert L. 1964 Steady and unsteady motions and wakes of freely falling disks. *The Physics of Fluids* **7** (2), 197–208.

Wu, J-S & Faeth, Gerard M 1993 Sphere wakes in still surroundings at intermediate Reynolds numbers. *AIAA journal* **31** (8), 1448–1455.

Wu, Jie-Zhi, Ma, Hui-Yang & Zhou, M-D 2006 *Vorticity and vortex dynamics*. Springer Science & Business Media.

Zhou, J., Adrian, R. J., Balachandar, S. & Kendall, T. M. 1999 Mechanisms for generating coherent packets of hairpin vortices in channel flow. *Journal of Fluid Mechanics* **387**, 353–396.